INFLUENCE OF ELECTROLYTE COMPOSITION AND TEMPERATURE ON ENERGY DEMAND AND ZINC STRUCTURE DURING ELECTRO-GALVANIZING

Marc Debeaux, Marco Witte, Thomas Koll – Salzgitter Mannesmann Forschung GmbH, Germany

ABSTRACT

The energy demand for the zinc deposition during electro-galvanizing is mainly composed of the cell voltage and the cathodic current efficiency. The influence of electrolyte composition and temperature on current efficiency and energy demand has been investigated in literature for low current densities of up to 5 A/dm². However, there are only a few studies on the behaviour of current efficiency with higher current densities. In this contribution, the influence of the electrolyte composition and temperature on cathodic current efficiency and cell voltage for relevant current densities are investigated. For this purpose, laboratory tests are carried out in a flow cell. The results are translated into an overall model that allows to estimate the total energy consumption. Furthermore, the resulting zinc coatings are analysed in terms of zinc adhesion, morphology, and zinc crystallography.

KEYWORDS

electro-galvanizing, corrosion protection, conductivity, current efficiency, texture analysis

INTRODUCTION

The electro-galvanizing of steel strip represents an important industrial process of corrosion protection and surface finishing. Electro-galvanized steel sheets are used e.g. in the automotive industry, for household appliances, and in the electronics industry. The zinc coatings show a very homogenous microstructure, a good spot weldability, as well as excellent surface appearance and painting adhesion properties [1].

In contrast to hot-dip galvanizing, zinc layers with a thickness below 3 µm or single-side coatings are easily feasible with the electro-galvanizing process. Furthermore, the influence of alloying elements in the steel substrate on both surface quality and zinc adhesion is comparably low when zinc is applied by electrolysis. Therefore, electro-galvanizing is interesting for corrosion protection of high alloyed steel sheets [1]. However, the energy demand for this process is high. High current densities are needed to enable fast and economical production. Although even higher current densities have been shown [2], current densities up to 200 A/dm^2 are used in practice for the electro-galvanizing process [3].

For the continuous zinc plating of steel strip, electrolytes based on sulfuric acid are used frequently. These electrolytes are highly acidic (pH = 1) to slightly acidic (pH = 3.5) [4] and typically result in cathodic current efficiencies of above 95% [5]. Sufficient electrolyte flow is needed to avoid current densities close to the limiting current density (i_{lim}) and thus preventing formation of dendrites or powdery zinc deposits [6]. This can be achieved by different cell designs (vertical, horizontal, radial) with forced electrolyte flow [4].

The influence of electrolyte composition and temperature on current efficiency and energy demand has been investigated for current densities of up to 5 A/dm^2. Here, an energy demand between 650

and 720 kJ/mol was found for the electrowinning process [7–9]. However, there are very few studies on the behaviour of current efficiency during the electro-galvanizing process. Weymeersch et al. [10,11] have studied different electrolyte compositions based on sulfuric acid with the following results:

- The higher the flow velocity, the higher the current efficiency.
- For high flow velocities the current efficiency is nearly independent from current density.
- The highest current efficiencies are found for high temperatures and high current densities.

In this contribution, the influence of electrolyte composition and temperature on cathodic current efficiency and cell voltage are investigated. The results are translated into an overall model that allows to estimate the total energy consumption. Furthermore, the resulting zinc coatings are analysed in terms of zinc adhesion, morphology, and zinc crystallography.

1. EXPERIMENTAL

The number of experiments was reduced by making use of design of experiments (DoE). For this purpose, a Face-Centered-Composite Design (FCCCD) was applied. For the analysis of the data, regression models were employed using linear, quadratic, and interaction terms of two parameters according to the general formula:

$$y = c_0 + \sum_{i=1}^{n_f} c_i\, x_i + \sum_{i=1}^{n_f} c_i x_i^2 + \sum_{i=1}^{n_f-1} \sum_{j=i+1}^{n_f} c_{ij} x_i x_j \qquad (1)$$

For the experiments the parameters pH, sodium (γ_{Na}), and zinc (γ_{Zn}) concentrations as well as the electrolyte temperature (ϑ) were varied. The actual concentrations are given in Table 1.

For the galvanizing experiments, electro-galvanized cold rolled deep drawing steel sheets (dimensions: 1.9×1.3 dm^2; thickness: 1.0 mm; chemical analysis in wt.%: C 0.0044, Si 0.018, Mn 0.116, P 0.007, Ti 0.0766) textured with a structured hard-chromed skin-pass roll [12] (Salzgitter Flachstahl GmbH, Germany) were used. Electro-galvanized material was used as reference material to allow a longer storage time during the course of the investigation. The specimens were degreased with alkaline solution. The existing zinc layer was removed by pickling in sulphuric acid (200 g/L) at room temperature. After the stop of hydrogen evolution, the specimens were left for another 10 s in the pickling acid. After that, the specimens were thoroughly rinsed with deionized water and directly inserted into the galvanic flow cell. For the preparation of synthetic electrolytes, zinc sulphate heptahydrate, sodium hydroxide, anhydrous sodium sulphate, and sulfuric acid (95% w/w) were used in p. a. grades. As standards for the calibration of pH conductivity measurements commercially available solutions were used.

The galvanizing experiments were carried out in an electro-galvanizing simulator (Fig. 1) equipped with a vertical (upstream) flow cell using two parallel working EA-PS-8040-340 galvanostats (Elektro-Automatik GmbH & Co. KG, Viersen, Germany). The plating was done simultaneously at both sample sides with a constant current. Insoluble anodes made from titanium with MMO coating (mixed metal oxide) were used. The anode-sample gaps were 5 mm each, the deposition area 1.7 dm^2 for each side. The electrolyte flow velocity (v) was set to 3 m/s within the flow cell. A current density of 70 A/dm^2 was used for each sample side. The plating time was 21 s. Electrolyte temperature was measured with a Pt100 element (Mazurczak GmbH, Germany). The time between starting the pump and the begin of the electrolysis was 10 s in order to homogenize the electrolyte flow. After plating,

the samples were thoroughly rinsed with deionized water and dried with a compressed air stream. Mean values of electrolyte temperatures and cell voltages over plating time were used for the analysis. Cell voltages were considered independently for each sample side. Five samples were produced for each parameter set according to Table 1.

Table 1: Dependency of electrolyte composition and temperature on conductivity σ, cell voltage U_{cell} and cathodic current efficiency η_c, as well as exemplary energy consumptions E/n calculated with eq. (5) (U_{cell} is given as mean values for both sample sides; the electrolyte conductivity is given directly before plating; *the marked electrolytes indicate the four basic electrolytes)

No.	pH	γ_{Zn} / g/L	γ_{Na} / g/L	ϑ / °C	σ / mS/cm	U_{cell} / V	η_c / %	E/n / MJ/mol
1*	2.02	61	0	49.7	71.9	8.82	99.2	1.72
2	2.02	61	0	64.2	84.0	7.92	99.1	1.54
3	1.00	61	0	50.1	117.2	6.65	97.1	1.32
4	1.00	61	0	65.1	127.8	6.29	98.9	1.23
5	1.49	58	27.3	56.9	148.0	5.85	98.4	1.15
6	1.96	52	44.5	50.3	150.0	5.90	98.6	1.15
7	1.96	52	44.5	65.2	185.7	5.28	99.0	1.03
8	1.02	52	44.5	50.0	184.5	5.42	95.7	1.09
9	1.02	52	43.7	65.2	217.0	4.98	97.8	0.98
10*	1.51	81	43.7	57.3	96.6	7.22	99.7	1.40
11	2.03	79	0	57.4	133.1	6.17	99.6	1.20
12	1.50	79	23.9	49.9	126.4	6.37	99.5	1.24
13	1.50	79	23.6	57.2	141.3	6.00	99.3	1.17
14*	1.50	82	23.6	50.2	126.7	6.36	99.3	1.24
15	1.50	82	22.9	57.5	141.1	6.02	99.6	1.17
16	1.50	82	22.9	64.8	157.5	5.77	99.6	1.12
17	1.00	80	23.7	57.4	160.8	5.65	99.3	1.10
18	1.53	79	44.0	57.5	107.2	5.55	99.5	1.08
19*	1.95	99	0	49.9	88.1	7.78	100.0	1.50
20	1.95	99	0	64.4	106.2	6.99	99.9	1.35
21	1.00	97	0	50.4	120.0	6.58	99.5	1.28
22	1.00	97	0	64.4	136.5	6.05	99.6	1.17
23	1.52	94	23.8	57.2	140.9	6.05	99.7	1.17
24	2.01	92	43.4	50.4	137.9	6.16	100.0	1.19
25	2.01	92	43.4	64.8	177.5	5.49	100.0	1.06
26	1.02	90	41.9	50.3	161.2	5.80	96.7	1.16
27	1.02	90	41.9	64.6	195.1	5.03	99.5	0.98

To reduce the number of different electrolytes (50 L of volume) an optimized experimental procedure was developed (Table 1). For a given zinc concentration, zinc sulphate and sodium sulphate were dissolved in deionized water at room temperature under stirring. The pH value was adjusted at room temperature by addition of sulfuric acid in well stirred solutions. Further combinations of sodium concentration and pH value were set by adding sodium sulphate, sodium hydroxide and/or sulfuric acid to the previous electrolyte. In total four basic electrolytes were used (Table 1). pH measurements were performed at room temperature using a pH 95 (WTW GmbH, Germany). Electrolyte conductivity was measured with a LF 197 (WTW GmbH, Germany) using a TetraCon35 standard conductivity cell (WTW GmbH, Germany) at process temperature without temperature compensation before and after each sample plating. The electrolyte composition was determined by ICP-OES analysis (Table 2).

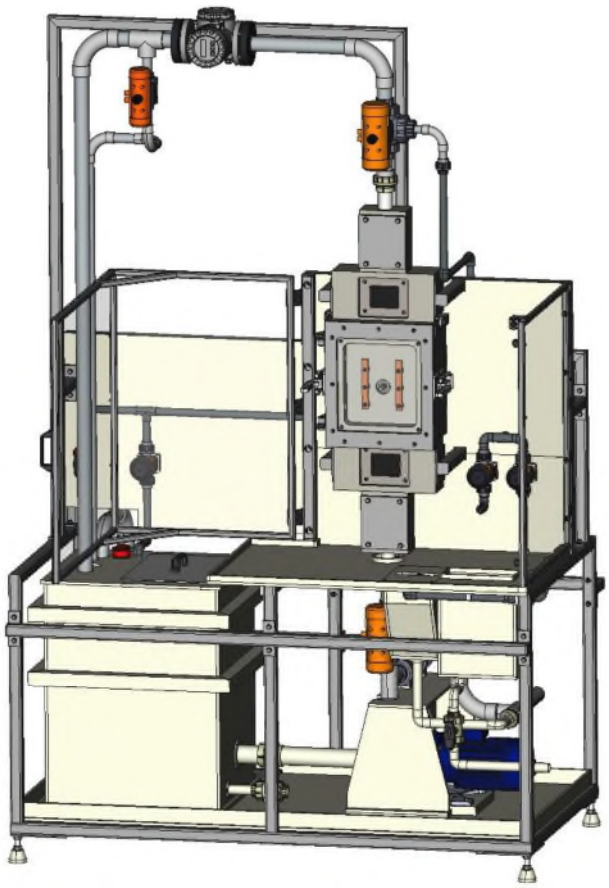

Fig. 1: Electro-galvanizing simulator at SZMF

For the determination of cathodic current efficiency, the zinc layer was stripped with an aqueous solution of hydrochloric acid (50% v/v) and 3.5 g/L hexamethylenetetramine as an inhibitor. The samples were thoroughly rinsed with deionized water in three steps and finally with ethanol and then dried with warm air stream. Zinc mass was determined by differential weighing on three samples for each parameter set.

Scanning electron microscopy (SEM) images were obtained on a Supra 55VP (Carl Zeiss, Germany) equipped with a SUTW 3.3 (EDAX, USA) EDX detector. To study the effect of the different coating conditions on the zinc textures, incomplete pole figures were measured with a D8 Discover X-ray diffractometer (Bruker, Germany) equipped with a Vantec2000 area detector using $Fe_{K\alpha}$ radiation. To avoid overlap with X-ray peaks of the steel substrate and remnant $Fe_{K\beta}$ zinc peaks, only pole figures of the {002}-, {101}-, {102}-, and {004}-peaks were measured. Although the {002}- and {004}-peaks have identical pole figures, they were still used for the texture calculations for improved measurement statistics. Orientation density functions (ODFs) were derived from the experimental pole figures with the Matlab® toolbox MTEX [13].

Zinc adhesion was tested with a glue bead test (according to BMW AA-0509). Samples of 200×30 mm^2 (perpendicular to direction of rolling) were cut and degreased with *n*-heptane. A structural adhesive (Betamate 1496V, Dow Automotive AG, Germany) was then applied in the dimensions of 4.0–5.0 mm thickness and 100.0 mm width at 50 °C. The adhesive was cured at 175 °C for 25 min. After 1 d of storage the samples were bent to an angle of about 90° (glue bead at the outer side). The fracture pattern was assessed visually (delaminating, cohesive, or adhesive fracture).

2. RESULTS AND DISCUSSION

The results of the individual experiments are summarised in Table 1. Here, mean values of five (conductivity and cell voltage) or three (cathodic current efficiency) independent experiments are given for an overview. However, for the calculation of the regression models all the individual data sets that were available were used.

Actual temperatures during conductivity measurements were used for regression analysis of the electrolyte conductivity. By applying the model given in eq. (1) the factors summarized in Table 2 were obtained with a good correlation (cor. $R^2 = 0.95$). As expected, the highest values for the conductivity were found for the combination of high temperatures and high sodium concentrations as well as low pH values.

Table 2: Results of the empiric regression models

parameter	σ / mS/cm	U_{cell} / V	η_c / %	E/n / kJ/mol
pH	–133	4.16	10.3	603
γ_{Zn}	$-5.34\cdot10^{-1}$	$8.91\cdot10^{-3}$	$2.79\cdot10^{-1}$	1.36
γ_{Na}	4.54	$-6.36\cdot10^{-2}$	$-8.61\cdot10^{-2}$	–13.2
ϑ	$3.76\cdot10^{-2}$	$-1.21\cdot10^{-1}$	$3.30\cdot10^{-1}$	–22.3
pH^2	27.9	$-3.17\cdot10^{-1}$	$-6.62\cdot10^{-1}$	–26.0
γ_{Zn}^2	$-2.75\cdot10^{-4}$	$3.61\cdot10^{-5}$	$-1.20\cdot10^{-3}$	$2.14\cdot10^{-1}$
γ_{Na}^2	$-5.14\cdot10^{-3}$	$6.71\cdot10^{-4}$	$-9.61\cdot10^{-5}$	$1.33\cdot10^{-1}$
ϑ^2	$9.38\cdot10^{-3}$	$1.02\cdot10^{-3}$	$-7.52\cdot10^{-4}$	$1.68\cdot10^{-1}$
$pH \cdot \gamma_{Zn}$	$2.62\cdot10^{-1}$	$-1.07\cdot10^{-2}$	$-1.31\cdot10^{-2}$	–2.51
$pH \cdot \gamma_{Na}$	$1.17\cdot10^{-1}$	$-2.67\cdot10^{-2}$	$-4.21\cdot10^{-4}$	–5.01
$pH \cdot \vartheta$	$-0.149\cdot10^{-1}$	$-1.57\cdot10^{-2}$	$-1.16\cdot10^{-1}$	–1.22
$\gamma_{Zn} \cdot \gamma_{Na}$	$-2.47\cdot10^{-2}$	$4.72\cdot10^{-4}$	$-4.21\cdot10^{-4}$	$8.41\cdot10^{-2}$
$\gamma_{Zn} \cdot \vartheta$	$9.26\cdot10^{-3}$	$-2.16\cdot10^{-4}$	$-6.31\cdot10^{-4}$	$-6.10\cdot10^{-2}$
$\gamma_{Na} \cdot \vartheta$	$-9.84\cdot10^{-3}$	$1.52\cdot10^{-5}$	$1.27\cdot10^{-3}$	$2.05\cdot10^{-2}$
const.	186	7.86	69.1	1700
cor. R^2	0.95	0.98	0.82	0.83

Furthermore, the conductivity seems to be increasing for decreasing zinc concentrations. This fact could be attributed to viscosity changes. Therefore, for all electrolytes the densities and dynamic viscosities were determined at the corresponding temperatures. However, a simple connection between conductivity, viscosity, and zinc concentration could not be found.

For the correlation of the cell voltage with the electrolyte composition, mean values of the cell voltage during the zinc deposition were used. The results of the correlation analysis are summarized in Table *2*. In sum, a high correlation of the cell voltage to the electrolyte composition and temperature was received (cor. $R^2 = 0.98$).

The correlation between electrolyte conductivity and cell voltage is given by Ohm's law. The measured cell voltage consists of several different single voltage drops (e.g. leads, connectors, electrolyte medium). For the present experiments only the resistance of the electrolyte medium (composition and temperature) was varied. Therefore, the cell voltage U_{cell} can be described as a function of electrolyte conductivity σ, anode-sample distance l and current density i. Here, U_{el} is the voltage drop from ohmic electrolyte resistance and U_0 is a system property.

$$U_{cell} = U_0 + U_{el} = U_0 + \frac{l \cdot i}{\sigma} \qquad (2)$$

Because anode-sample distance (= 5 mm) and current density (= 70 A/dm^2) were fixed, the voltage drop U_0 can be determined from a regression analysis. This was done independently for the two individual sample sides (front: 3.48 V, back: 3.66 V) of each sample with a good correlation (R^2 = 0.97) in both cases (Fig. 2). The higher voltage drop on the back side of the sample could be ascribed to a slightly higher resistance for the contacting (additional connectors) or to a small deviation of the precise sample position between the two anodes.

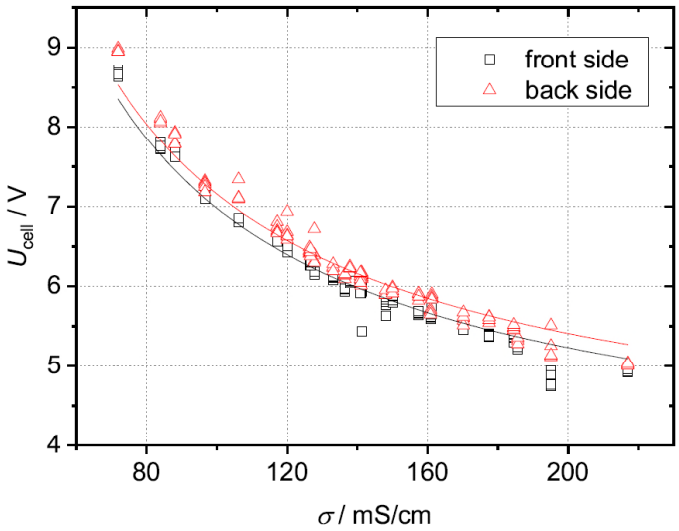

Fig. 2:Voltage drop as a function of electrolyte conductivity

The cathodic current efficiency is the ratio of the actual mass to the theoretical mass liberated to Faraday's law (eq. 3). It is decreased by electrochemical reduction of hydroxonium ions to atomic hydrogen as a side reaction on the cathode [14].

$$\eta_c = \frac{m_{effective}}{m_{theo}} \tag{3}$$

Three samples of each parameter set were used for calculating the regression model of the cathodic current efficiency mean values. In this case the correlation had a poorer quality (cor. R^2 = 0.82). This can be attributed to relatively small differences in the current efficiency. In total, high values (>96%) for the current efficiency were found. In three cases (samples 19, 24, 25) the current efficiency was found to be very close to 100%. In summary, a strong dependency of zinc concentration and temperature was observed.

To find the optimal combination of all parameter sets for low energy requirements it is important to simultaneously look at both cell voltages and current efficiencies. If a low cell voltage is obtained by a suitable combination of electrolyte composition and/or process variables, a low current efficiency could even reverse the energy demand for a given zinc layer thickness.

With Faraday's law and the definition for cathodic current efficiency eq. (3) the electric work E for the overall process of the electrodeposition can be calculated.

$$E = \frac{U \cdot I \cdot t}{\eta_c} = \frac{U \cdot n \cdot z \cdot F}{\eta_c} \tag{4}$$

Here, z is the charge of zinc (z = 2), n is the amount of substance and F is the Faraday constant. Considering eq. (2) the overall energy E per mole of deposited zinc is then:

$$\frac{E}{n} = \frac{2 \cdot U_{cell} \cdot F}{\eta_c} \quad \text{or} \quad \frac{E}{n} = \frac{2 \cdot \left(U_0 + \frac{l \cdot i}{\sigma}\right) \cdot F}{\eta_c} \tag{5}$$

Because current densities and resulting thicknesses have not been changed during the experiments, the relative energy demand could only be calculated for the given parameter space. Furthermore, electrolyte velocity and its influence on cathodic current efficiency has not been considered yet.

On basis of the results of both cell voltages and current efficiencies the energy demand can then be calculated according to eq. (5) (Table 1) and transferred into a regression model (Table 2). In Fig. 3 the contour plot representation of the energy consumption per mole is shown.

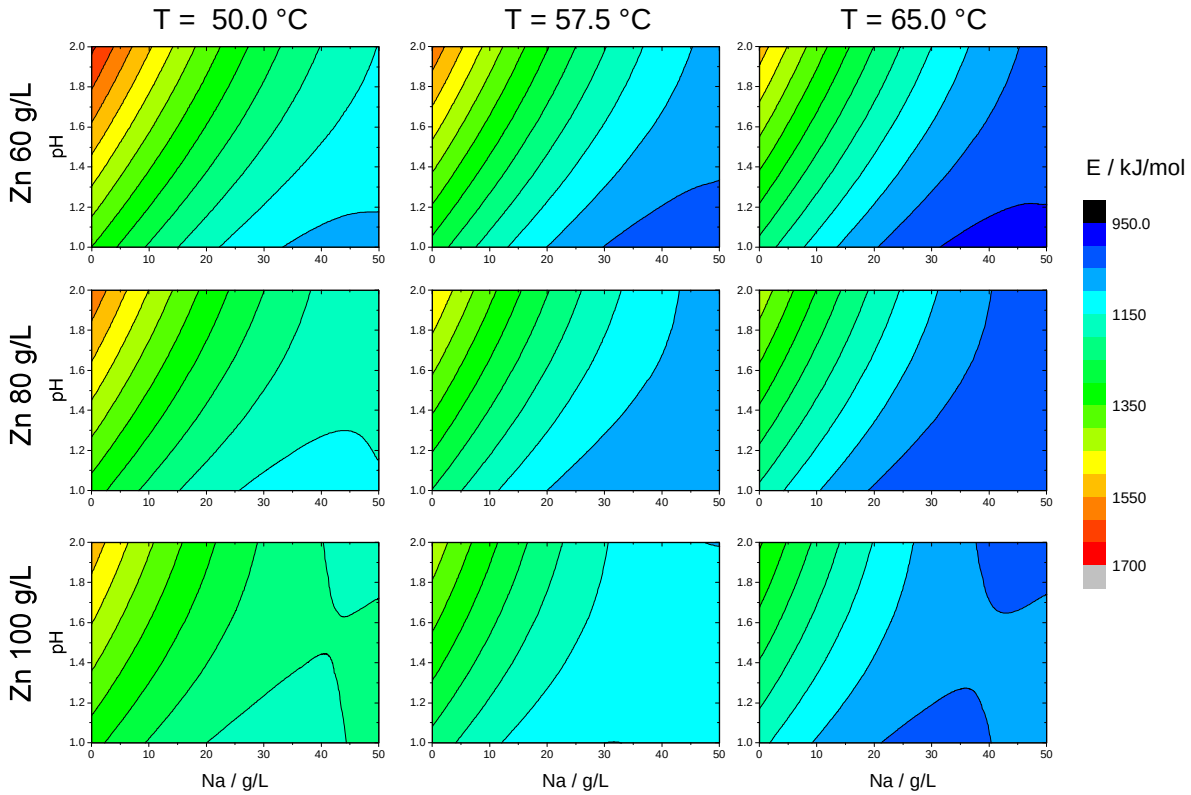

Fig. 3: Contour plot representation of the overall energy demand (d = 5 mm, v = 3 m/s, i = 70 A/dm^2)

For a given current density of 70 A/dm^2 and a flow velocity of 3 m/s the energy for deposition within the parameter space ranges between 980 and 1,660 kJ/mol. The higher the sodium concentration and the electrolyte temperature, the lower is the energy demand. Zinc concentration seems to have minor or negligible effects.

3. COATING CHARACTERIZATION

Zinc adhesion was tested for each sample series and was found to be excellent in every single case. In Fig. 4 SEM micrographs of zinc surfaces on selected samples (samples 1, 9, 13, 19, 27) are shown. All samples exhibit fully closed and well-formed zinc layers with different crystal morphologies. Therefore, the zinc textures were analysed intensively.

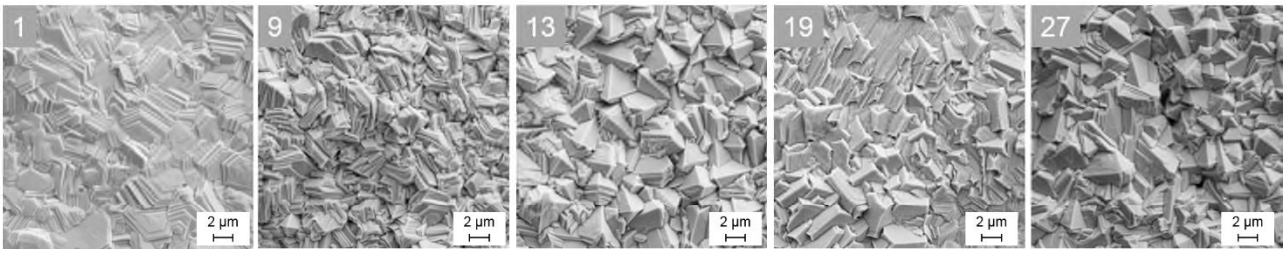

Fig. 4: SEM micrographs of selected zinc surfaces (magnification ×3,000)

Two examples of measured ODFs are shown in Fig. 5 as ϕ_2-sections. Sample 1 (Fig. 5a) shows a basal texture fibre ($< 0001 >$ || normal direction (ND)). The basal texture of sample 13 (Fig. 5b) is much weaker and it also contains a fibre of pyramidal type ($< \bar{1}2\bar{1}3 >$ || ND). An overview of the relevant zinc texture fibres is given in Fig. 6.

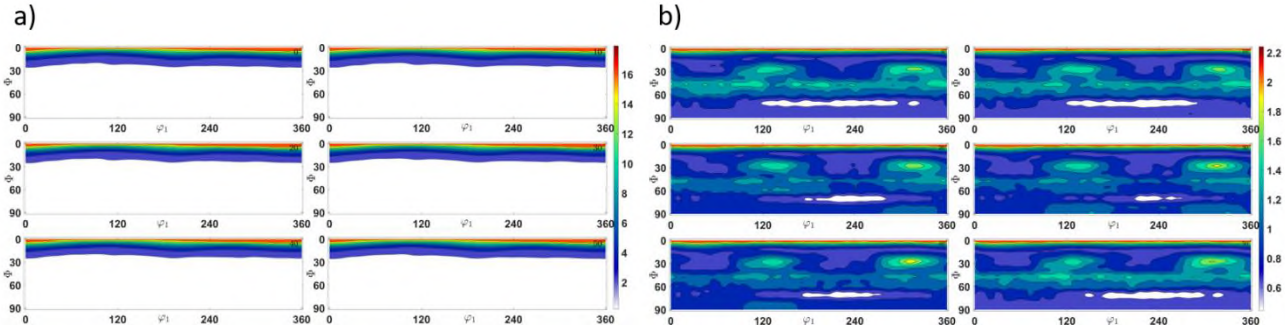

Fig. 5: ODF sections at ϕ_2 = 45° of samples 1 (a) and 13 (b)

The volume fraction $v(g)$ of a certain orientation g or a set of orientations g_i along a texture fibre can be derived from an ODF f via

$$v(g_i) = \int f(g_i)dg \tag{6}$$

For a correct comparison of such volume fractions also the multiplicity of texture fibres must be considered [15]. The multiplicities of the investigated fibres $< 0001 >$, $< 10\bar{1}0 >$, $< 10\bar{1}2 >$ and $< \bar{1}2\bar{1}3 >$ || ND are 2, 6, 12, and 12, respectively.

Calculated fibre fractions can only be compared to each other after they have been divided by their corresponding multiplicities. Fig. 6 shows the experimental fibre fractions normalized by their respective multiplicities. The samples 1 and 19 exhibit a pronounced basal $< 0001 >$ || ND fibre, while the other samples have a more random texture. This difference in crystallographic texture is also seen in the SEM micrographs in Fig. 4. The samples with basal texture show a smoother surface with tile-like structures, while the samples with random texture yield a surface dominated by pyramidal features. The samples with basal texture are those with a low electrolyte conductivity. A smoother surface of a zinc layer with basal textures has also been observed by Nakano et al. [16]. Furthermore, it could be confirmed that samples with a higher degree of basal textures show an increased lightness and gloss, which could be ascribed to increased smoothness [17].

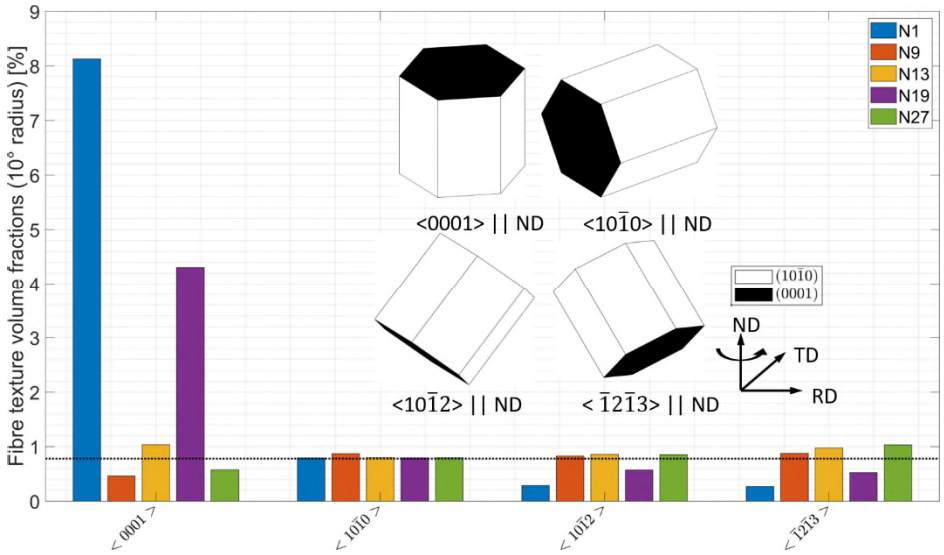

Fig. 6: Fibre volume fractions calculated from the ODF and normalized by their multiplicities and orientation of the zinc elemental crystal cells for typical zinc fibre textures along the sheet normal direction. The dashed line represents the fibre volume fraction of a random texture. (ND = normal direction, TD = transverse direction, RD = rolling direction of the steel sheet)

4. CONCLUSIONS

The energy demand depending on electrolyte composition and temperature for the electro-galvanizing process under a certain current density (70 A/dm^2), a quiet small anode-cathode distance (5 mm) and for an identical deposition time (21 s) was investigated intensively and a simple model was developed. Here, the lowest energy demand within the parameter space with about 980 kJ/mol was found for a high electrolyte temperature (65 °C), a high sodium concentration (50 g/l), a low pH value (1.0), and a low zinc concentration (60 g/l). On the other hand, the highest energy demand within the parameter space with about 1660 kJ/mol was found for a low electrolyte temperature (50 °C), a low sodium concentration (0 g/l), a high pH value (2.0), and a low zinc concentration (60 g/l). It has been shown that zinc growth could be altered significantly without varying current density. It is known that different crystallographic textures of zinc coatings could affect their corrosion and mechanical properties [18]. In the context of this study, however, this was not the focus and has not been further investigated.

However, real conditions in electro-galvanizing lines are much more complex than it could be shown in this study. Above all, current densities in the industrial process are varying because of different desired layer thicknesses and line speeds. Depending on cell design, current densities could also vary locally under certain circumstances in the plant (e.g. by non-parallel anodes) [19]. In addition, the influence of accompanying elements in the electrolyte, especially iron with its two oxidation states, should be considered in further studies. Iron could lower the cathodic current efficiency and therefore plays an important role [20].

Furthermore, in some areas of the galvanic section of electro-galvanizing lines the steel strip is outside an electric field (e.g. around sink rolls). This could locally result in re-dissolution processes (by pickling) that may reduce the apparent current efficiency and therefore increase energy demand. The pickling activity of the electrolyte is a function of electrolyte composition, its temperature, and local flow conditions. Finally, it is also known that the rectifiers have an optimum working range depending on nominal voltage. Working at non-optimal operating points could have a negative effect on possible energy savings [19].

ACKNOWLEDGEMENTS

We thank the European Commission and the Research Fund for Coal and Steel for funding (RFSR-CT-2013-00009) and our project partners for fruitful discussions and support. For these studies we would like to especially thank De Nora Deutschland GmbH for providing anode samples and VDEh-Betriebsforschungsinstitut GmbH (BFI) for performing viscosity measurements. Special thanks go to Sebastian Richter for his contribution during his bachelor thesis.

REFERENCES

1) W. KARNER, T. LAVRIC, J. GERDENITSCH, J. FADERL, S. WIESINGER, Galvatech, Genova (2011).
2) R. WINAND, Galvatech, Tokyo (1989).
3) J. H. LINDSAY, T. J. O'KEEFE, Electrogalvanizing, Springer Science (1994), p. 165.
4) R. WINAND, Electrodeposition of Zinc and Zinc Alloys, John Wiley & Sons (2010), p. 285.
5) R. WINAND, J. Appl. Electrochem. 21, (1991), p. 377.
6) L. N. BENGOA, S. BRUNO, H. A. LAZZARINO, P. R. SER, W. A. EGLI, J. Appl. Electrochem. 44, (2014), p. 1261.
7) A. M. ALFANTAZI, D. B. DREISINGER, J. Appl. Electrochem. 31, (2001), p. 641.
8) T. J. TUAWERI, E. M. ADIGIO, P. P. JOMBO, Int. J. Eng. Sci. Invent. 2, (2013), p. 17.
9) M. BESTETTI, U. DUCATI, G. H. KELSALL, G. LI, E. GUERRA, Can. Metall. Quart. 40, (2001), p. 451.
10) A. WEYMEERSCH, R. WINAND, L. RENARD, Plat. Surf. Finish., (1981), p. 56.
11) A. WEYMEERSCH, R. WINAND, L. RENARD, Plat. Surf. Finish., (1981), p. 118.
12) W. ZIMNIK, B. RITTERBACH, K. MÜLL, O. SCHANDERL, Asia-Pacific Galvanizing Conference, Korea (2009).
13) R. HIELSCHER, H. SCHAEBEN, J. Appl. Crystallogr. 41, (2008), p. 1024.
14) D. R. GABE, J. Appl. Electrochem. 27, (1997), p. 908.
15) J. HANSEN, J. POSPIECH, K. LÜCKE, Tables for Texture Analysis of Cubic Crystals, Springer (1978).
16) H. NAKANO, S. OUE, S. TANIGUCHI, S. KOBAYASHI, H. FUKUSHIMA, ISIJ Int. 48, (2008), p. 634.
17) H. KAWANO, S. OUE, T. FUTABA, A. KOBAYASHI, Y. GOTO, H. NAKANO, ISIJ Int. 58, (2018), p. 2117.
18) P. SER, J. CULCASI, C. ELSNER, A. D. SARLI, Surf. Coat. Tech. 122, (1999), p. 143.
19) A. BÁN, R. WOLTERS, A. BUTTLER, H. BERENDS, T. LAVRIC, A. CALDERARA, F. TIMPANO, T. FURUSAWA, M. DEBEAUX, T. KOLL, J. GERDENITSCH, Energy and resource efficient electro-galvanizing of steel strip (EfficientELO), Tech. rep., European Commission, RFCS, (2017).
20) V. F. C. LINS, ABELHA, R., M. M. M. DE CASTRO, M. M. D. DE SOUZA, L. L. DE MORARES, C. R. ARAÚJO, T. MATENCIO, Tecnol. Metal. Mater. Min. 7, (2010), p. 61.